Chemical Science

EDGE ARTICLE

View Article Online
View Journal | View Issue

Cite this: *Chem. Sci.*, 2020, **11**, 113

All publication charges for this article have been paid for by the Royal Society of Chemistry

Reaction mechanism, norbornene and ligand effects, and origins of *meta*-selectivity of Pd/norbornene-catalyzed C–H activation†

Tao Yang, *[a] Chuncai Kong, [a] Shengchun Yang, [a] Zhimao Yang,[a] Sen Yang[a] and Masahiro Ehara *[bc]

The reaction mechanism, ligand and norbornene effects, and origins of *meta*-selectivity in Pd/norbornene-catalyzed alkylation and arylation *via* C–H activation are theoretically elucidated by DFT computation. The reaction proceeds through six major steps: *ortho*-C–H activation, norbornene insertion into Pd–C bonds, *meta*-C–H activation, *meta*-C–C bond formation, β-carbon elimination, and protodemetallation. Both *ortho*-C–H and *meta*-C–H activations undergo a concerted metalation–deprotonation pathway. The *meta*-C–C bond formation, which is the selectivity-determining step, follows a Pd(IV) pathway *via* oxidative addition on a Pd(II) five-membered-ring intermediate. The oxidative addition of alkyl iodide adopts an S_N2 pathway, whereas aryl iodide prefers concerted oxidative addition rather than the S_N2 pathway. The Pd(II) pathway *via meta*-C–C reductive coupling on dinuclear palladium species is not the dominant pathway because of the low concentration of Pd(0)L_2. For methylation, with norbornene and pyridine (or its derivative) as ligands, the C–C reductive coupling and C–C reductive elimination from the Pd(IV) intermediate are found to be the selectivity-determining steps for *meta*-functionalization and benzocyclobutene formation, respectively, whereas the use of large ligands such as acridine and quinoline-type ligands (**L1** and **L2**) moves the selectivity-determining step back to the oxidative addition and the C–C reductive elimination steps on the Pd(II) intermediate. The geometric and electronic properties of **L1** and **L2** further suppress the benzocyclobutene formation by increasing the energy difference between *meta*-functionalization and benzocyclobutene formation. The combination of 2-carbomethoxynorbornene and **L2** promotes *meta*-ethylation and -arylation by disfavoring the C–C reductive elimination steps from the Pd(II) and Pd(IV) intermediates as well as slightly favoring the oxidative addition step.

Received 19th September 2019
Accepted 22nd October 2019

DOI: 10.1039/c9sc04720d

rsc.li/chemical-science

Introduction

Direct C–H functionalization, which allows the conversion of C–H bonds to C–C or C–X bonds, has attracted wide interest as a powerful synthesis methodology in the past few decades.[1] Highly selective C–H functionalization of arenes which occurs *via* activation of the inert C–H bond can be utilized for various promising applications in many fields including pharmaceutical, agrochemical and materials industries.[2] However, achieving site selective C–H functionalization of arenes is still challenging, especially in the development of synthetically useful remote arene C–H activation. In particular, *meta*- and *para*-selective functionalizations have emerged as important targets very recently, because *ortho*-C–H functionalization methods have been extensively exploited.[2,3] Up to now, there are a limited number of available transition-metal-catalyzed *meta*-C–H functionalizations such as steric-controlled formal *meta*-C–H functionalization,[4] *meta*-C–H functionalization *via* traceless directing groups,[5] chelation-assisted *meta*-C–H arylation,[6] and *meta*-C–H functionalization utilizing nitrile-containing templates.[7]

Inspired by the Catellani reaction,[8,9] Yu's group developed a new approach for *meta*-selective C–H functionalization of arenes containing an amide-directing group (phenyl acetamides) by employing norbornene (**N1**) and a Pd(II) catalyst with pyridine-based ligand **L1** synthesized by their group (catalytic system **A**),[10] as shown in Scheme 1. The use of this catalyst switches *ortho*-selectivity to *meta*-selectivity and achieves the highly selective *meta*-alkylation and -arylation. More interestingly, modifying the norbornene (**N1**) to 2-carbomethoxynorbornene (**N2**) and changing the ligand **L1** to a quinoline-

[a]*School of Science, MOE Key Laboratory for Non-Equilibrium Synthesis and Modulation of Condensed Matter, Xi'an Jiaotong University, Xi'an 710049, Shaanxi, China. E-mail: taoyang1@xjtu.edu.cn*

[b]*Research Center for Computational Science, Institute for Molecular Science, Nishigonaka 38, Myodaiji, Okazaki 444-8585, Japan. E-mail: ehara@ims.ac.jp*

[c]*Elements Strategy Initiative for Catalysts and Batteries (ESICB), Kyoto University, Kyoto 615-8520, Japan*

† Electronic supplementary information (ESI) available. See DOI: 10.1039/c9sc04720d

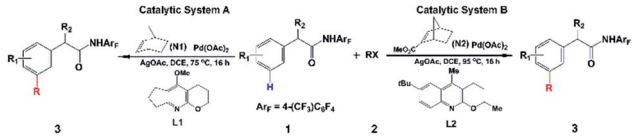

Scheme 1 Pd/norbornene-catalyzed *meta*-selective C–H activation of arenes.[9,10]

based ligand **L2** (catalytic system **B**), Yu and coworkers significantly improved the efficiency and scope of this *meta*-selective C–H functionalization.[11] For example, only functionalization of aryl iodides with either an *ortho*-coordinating group or multiple electron-withdrawing substituents could be achieved with catalytic system **A**, but the use of catalytic system **B** could overcome this limitation and a broad range of aryl iodides can be employed for the *meta*-arylation protocol. This synthesis strategy has been successfully extended to *meta*-C–H chlorination, amination, and alkynylation.[12] Almost simultaneously, Dong and coworkers reported a similar Pd/norbornene-catalyzed *meta*-arylation reaction with dimethylamine as the directing group and $AsPh_3$ as the ligand, which is also effective with the aryl iodides with *ortho*-coordinating groups.[13] Very recently, Yu's group further extended this approach and successfully realized remote enantioselective *meta*-C–H arylation and alkylation by using Pd and chiral 2-carbomethoxynorbornene.[14]

As shown in Scheme 2, the amide-directed *ortho*-C–H activation, forming the *ortho*-palladacycle **I**, was proposed to be the first step of the *meta*-C–H functionalization of phenyl acetamides. Then, norbornene inserts into the Pd–C bond of **I** followed by *meta*-C–H activation, producing palladacycle **II**. Subsequent reaction of **II** with a coupling partner (alkyl or aryl iodides) affords palladacycle **IV** with a functionalized *meta* position *via* intermediate **III**. This step, which is known as the key pathway of the Catellani process, usually contains oxidative addition, reductive elimination and β-carbon elimination. Final protodemetallation of the aryl–palladium bond delivers the desired product. Because of the presence of intermediates **I**, **II**, and **IV**, the side reactions including *ortho*-C–H functionalization, *ortho*,*meta*-C–H difunctionlization and C–C reductive elimination of palladacycle **II** to form benzocyclobutene can also take place. However, with the aid of the pyridine-based ligand **L1** or **L2**, *ortho*-functionalized and *ortho*,*meta*-difunctionalized products were not observed experimentally, and the benzocyclobutene formation was minimized.

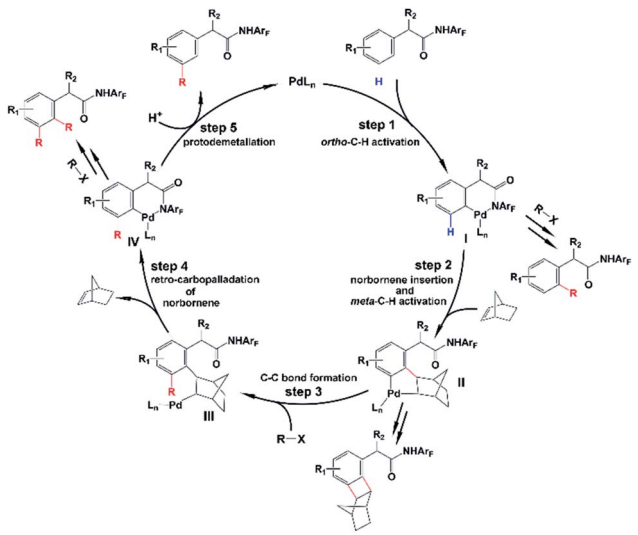

Scheme 2 Proposed mechanism for *meta*-selective C–H activation catalyzed by the Pd/norbornene system.

Even though the Pd/norbornene-catalyzed *meta*-C–H functionalization of phenyl acetamides has been well utilized experimentally, important questions have been unsolved. For example, the reaction mechanism is not clear, especially the transformation step from palladacycle **II** to **III** is completely uncertain. There are two different pathways proposed in the literature, the Pd(IV) pathway and Pd(II) pathway (also known as the transmetalation[15] pathway) which was proposed by Cardenas and Echavarren,[16] as shown in Scheme 3. The reaction pathway significantly depends on the reactant species. Previous mechanistic studies demonstrated that the Pd/norbornene-catalyzed reaction of metallacycles **II** with alkyl halides follows the Pd(IV) pathway *via* oxidative addition.[8a,17,18] However, for the aryl–aryl coupling, those two pathways could compete. By using an ethylene bridge to replace the norbornene unit, Cardenas and Echavarren performed theoretical calculations on simplified systems and revealed that the Pd(IV) pathway is favored over the Pd(II) pathway, which was also found by Wu and Lei.[16,19] Catellani and Derat theoretically confirmed that the intermediate palladacycle without *ortho*-substitution preferably undergoes the transmetalation pathway, whereas these palladacycles could probably undergo oxidative addition of an aryl halide when an *ortho*-substituent is present.[20] Moreover, the origins of selectivity of *meta*-C–H functionalization over other side reactions are not disclosed. Experimentalists need the knowledge about how much the ligand and norbornene influence the selectivity and scope of this reaction. However, the knowledge and answers for all these questions have not been presented at all.

The theoretical answers to the above open questions will undoubtedly deepen the understanding of the title reaction, assist in the design of more efficient and reactive norbornene and ligands, and promote further development of the *meta*-selective C–H functionalization methodology. In the present

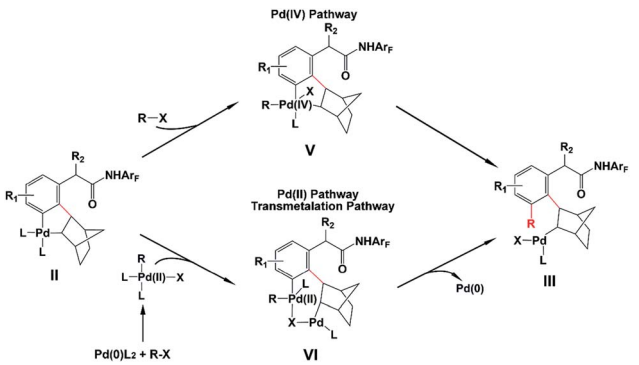

Scheme 3 Proposed pathways of the C–C bond formation step.

study, we performed theoretical calculations to elucidate the reaction mechanism, origins of selectivities, and effects of norbornene and ligands on palladium/norbornene-catalyzed amide-directed *meta*-selective C–H alkylation and arylation of phenyl acetamides.

Computational methods

All the structures were optimized in the gas phase by employing the ωB97XD functional[21] using the effective core potentials (Lanl2dz)[22] and basis sets for Ag, Pd and I and the 6-31G(d) basis set for all the other atoms. Frequency calculations were performed at the same level of theory to obtain zero-point vibrational energy and thermal corrections at three different temperatures, 348.15, 363.15, and 368.15 K, which were used experimentally. In the test calculations, the M06 [23] and B3LYP-D3 (Becke–Johnson damping, BJ)[24] results are very close to the ωB97XD ones.[25] Single-point energy calculations were carried out at the M06/SDD[26]-6-311++G(d,p) level, using the gas-phase optimized geometries, to evaluate electronic energies. This type of theoretical method has been frequently used in previous theoretical studies on Pd-catalyzed C–H activations.[27] Solvation free energy was calculated by using the SMD[28] model with two experimentally employed solvents, 1,2-dichloroethane (DCE) and trifluorotoluene ($PhCF_3$).[29] The partial charges were obtained from natural bond orbital (NBO)[30] analysis at the B3LYP/SDD-6-311++G(d,p)-SMD level. All theoretical calculations were conducted by employing the Gaussian 09 program.[31] Molecular structures were illustrated with CYLView.[32]

Results and discussion

Several pyridine-based ligands have been used experimentally.[10,11] When pyridine (Py) was used as the ligand, both the *meta*-functionalized product and benzocyclobutene were produced with the same yield. The ligands **L1** and **L2** were found experimentally to be better than pyridine and to significantly improve the yield of the *meta*-functionalized product. However, to clarify the possible competing pathways of catalytic cycles, pyridine is used as a ligand in calculations here, to save computation time.

1. Initiation and substrate binding

In 2014 Yu's group reported a pyridine-based ligand-promoted C(sp^3)–H activation and obtained a five-membered-ring cyclopalladation intermediate as crystals,[33] analogous to the six-membered-ring cyclopalladacycle **I**. Theoretical calculations by Wang *et al.* also confirmed that the catalytic cycle involving the five-membered-ring cyclopalladation intermediate is formed from square planar Pd(II) bis-ligated complexes.[34] On the basis of those results, both *trans* and *cis* square planar Pd(II) dipyridine complexes, which are formed from precatalyst $Pd_3(OAc)_6$, have been proposed, as shown in Fig. 1. Though the formation of the *cis*-form **2** is not exergonic, we will not rule out any of them in this stage.

The *N*-2,3,5,6-tetrafluoro-4-trifluoromethylphenylamide substrate (**1a**), which was derived from phenylacetic acid, was applied experimentally to the investigation of the ligand effect. Because the deprotonation reaction takes place with $\Delta G^\circ = -4.6$ kcal mol^{-1}, as shown in Scheme 4, three possible coordination modes such as a charge-neutral N-donor amide (**1a**), a deprotonated N-donor amidate anion (**1a′**) and, its resonance form, an O-donor imidate (**1a″**) are examined here. In a pre-catalyst **3** that is the isomer of the pre-catalyst **1**, the substitution of acetate for **1a′** occurs through a transition state **TS4** with a Gibbs activation energy ($\Delta G^{\circ\ddagger}$) of 25.3 kcal mol^{-1} and a Gibbs reaction energy (ΔG°) of 3.1 kcal mol^{-1}, as shown in Fig. 2, to afford Pd(OAc)(**1a′**)$(Py)_2$ **4**. However, the substitution reaction of

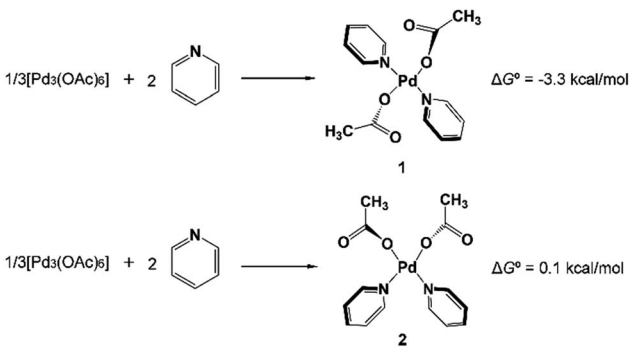

Fig. 1 Formation of the most stable *trans*-$PdPy_2(OAc)_2$ (**1**) and *cis*-$PdPy_2(OAc)_2$ (**2**).

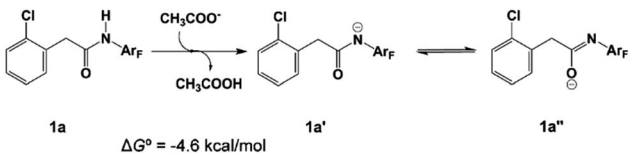

Scheme 4 The deprotonation reaction.

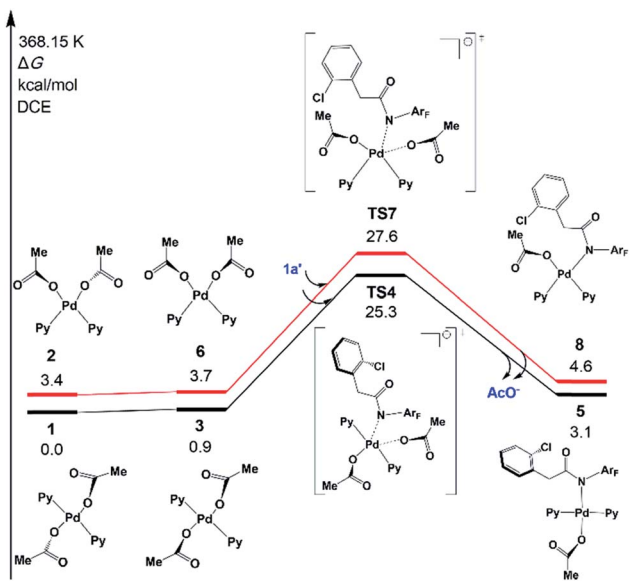

Fig. 2 Gibbs free energy profiles for the substitution reactions of **1** and **2** with **1a′**. Both *trans*- and *cis*-$Pd(Py)_2(OAc)_2$ pathways are included.

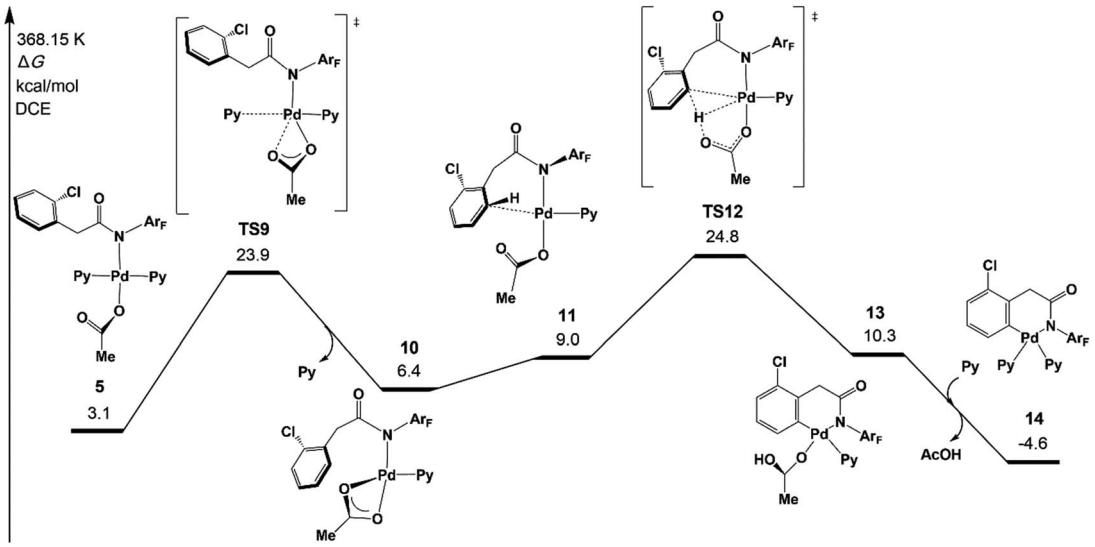

Fig. 3 Gibbs free energy profile for the concerted metalation–deprotonation (CMD) pathway of *ortho*-C–H activation.

1a and **1a**″ needs higher activation energy, indicating that **1a**′ is more reactive to form an active species than **1a** and **1a**″; see Fig. S1 and S2 in the ESI.†

A similar reaction that occurs from less stable *cis* complex **2** proceeds *via* a higher-energy transition state **TS7** ($\Delta G^{\circ\ddagger}$ = 27.6 kcal mol^{-1}) to afford complex **8** (ΔG° = 4.6 kcal mol^{-1}), indicating that **5** is preferably formed over **8**. Further examination revealed that through releasing one 2-pyridine ligand, both **5** and **8** could lead to the formation of the same bidentate carboxylate complex, which could undergo the *ortho*-C–H activation (Fig. S3†). The reaction mechanism that starts from **5** will be discussed in the following section.

2. *ortho*-C–H activation

Although the concerted metalation–deprotonation (CMD)[35] mechanism which is assisted by the acetate has been demonstrated to be a main C–H activation pathway, several other possible pathways were proposed in the previous mechanistic studies, including σ-bond metathesis and oxidative addition of the C–H bond.[7c] We investigated those three pathways and two new possible pathways, an AcOH-assisted CMD mechanism, in which AcOH plays a role in proton shuttle, and direct *ortho*-C–H activation *via* the CMD pathway, in which **1a** does not coordinate with Pd of **1** but reacts directly with *ortho*-C–H of **1** (see Fig. S4 in the ESI†).

The original CMD pathway was found to be the most favored mechanism among the five possible pathways, which agrees with previous mechanistic studies on palladium(II) acetate-catalyzed C–H activation reactions.[35] It is noteworthy that the direct CMD between complex **1a** and *trans*-Pd(Py)$_2$(OAc)$_2$ occurs at the *ortho*-C–H bond with a moderately higher activation energy than that of the original CMD pathway, indicating that the auxiliary additive might not be necessary for the reaction.[36] Very recently, Yu's group realized Pd/**N2**-catalyzed auxiliary-free *meta*-C–H arylation of phenylacetic acids with a pyridine-type ligand,[12f] which is consistent with the present calculation results.

Fig. 3 depicts the most favored CMD pathway of *ortho*-C–H activation with the Gibbs energy profile starting from **5**. The pathway starts from the attack of carboxylate oxygen on the Pd center and the dissociation of one pyridine ligand (**TS9**) occurs, resulting in a bidentate acetate intermediate **10**. Then, **10** isomerizes to an intermediate **11**, in which the *ortho*-C–H approaches the Pd center. No transition state has been located between **10** and **11**. Starting from **11**, the *ortho*-C–H bond of the phenyl group is activated and cleaved with the assistance of the bound acetate *via* **TS12** to afford an intermediate **13** with acetic acid being weakly bound to the Pd center. Further ligand exchange yields the six-membered-ring cyclopalladacycle **14**. *ortho*-C–H activation *via* **TS12** needs the highest $\Delta G^{\circ\ddagger}$ in the above steps but it is attainable at an energy of 24.8 kcal mol^{-1}. As shown in Fig. 4, the Pd–C distance in **TS12** becomes 2.121 Å and the H atom is transferred from the *ortho*-C to the acetate with C–H and O–H distances of 1.321 and 1.347 Å, respectively.

3. Norbornene insertion and *meta*-C–H activation

As shown in Fig. 5, there are two key steps in norbornene insertion. The first key step is to provide an empty coordination site for norbornene. This process occurs *via* the protonation

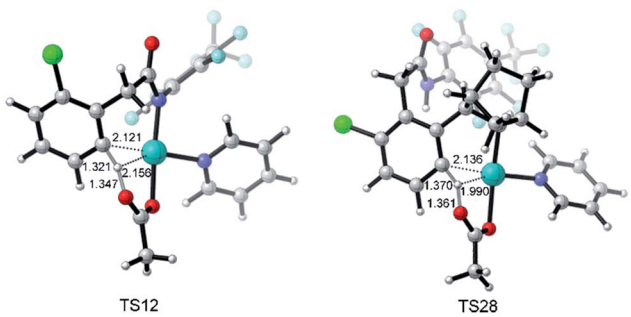

Fig. 4 Optimized structures of transition states **TS12** and **TS28** with selected distances given in angstroms.

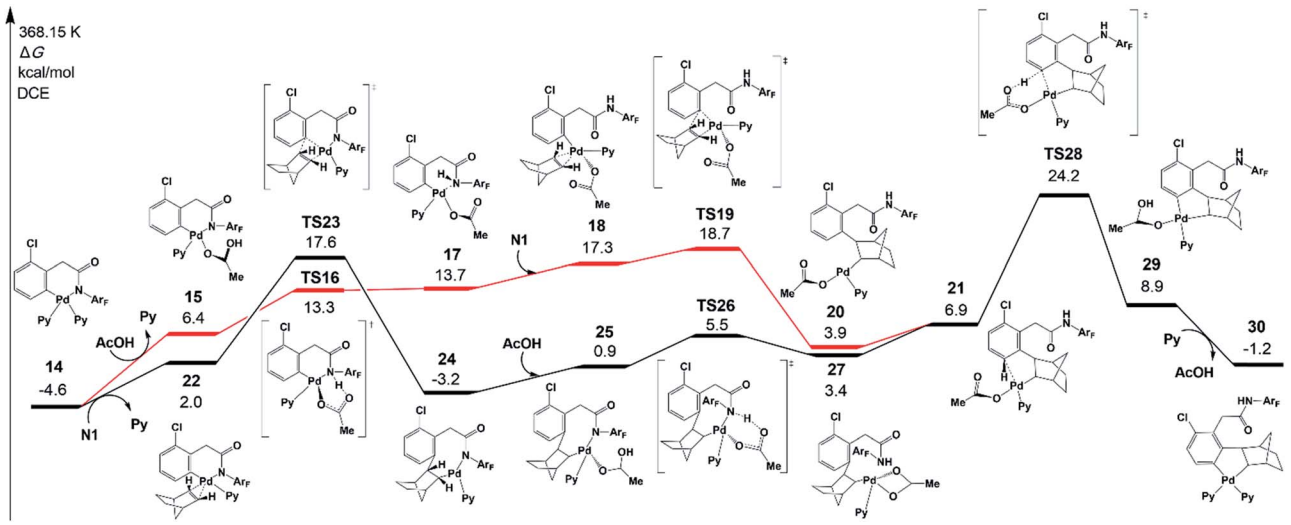

Fig. 5 Gibbs free energy profile for the norbornene insertion.

reaction of **14**, in which the weakly bound acetic acid protonates the amide auxiliary with the Pd–N bond scission (**TS16**). The protonation reaction affords an intermediate **17**, in which a weak interaction exists between Pd and N atoms. Because the Pd–N bond in **17** is weaker than in **14**, the $NHAr_F$ group easily dissociates from Pd followed by norbornene coordination to yield an intermediate **18**. The second key step is norbornene insertion *via* transition state **TS19**, which is the insertion of the norbornene double bond into the Pd–Ph bond to form an intermediate **20**. Then, **20** isomerizes to an intermediate **21**.

The highest-energy point in this pathway is **TS19**, which is 18.7 kcal mol^{-1} in energy. As shown by the black line in Fig. 5, there is another pathway that starts from norbornene insertion into the Pd–Ph bond *via* **TS23**, leading to intermediate **24**. After the coordination of AcOH to the Pd center (**25**), the protonation reaction takes place *via* **TS26** and the intermediate **27** is formed, followed by the isomerization to **21**. The highest-energy point in this pathway is norbornene *exo*-migratory insertion *via* **TS23** (17.6 kcal mol^{-1}),[38] revealing that this pathway is preferred. The *exo*-migratory insertion agrees with the experimental observation.[11]

Fig. 5 also presents the CMD pathway of *meta*-C–H activation, **TS28**, in which the *meta*-C–H bond cleavage occurs with the aid of the acetate, with an activation energy of 24.2 kcal mol^{-1}. Then, a five-membered-ring cyclopalladation intermediate **29** with weakly bound acetic acid is afforded. Further ligand exchange generates intermediate **30**.[37] Several other possible *meta*-C–H activation pathways, such as the oxidative addition of the C–H bond and an AcOH-assisted CMD pathway, have also been examined (Fig. S5†). However, they need larger activation energy, compared with the CMD pathway shown in Fig. 5. As shown in Fig. 4, the Pd–$H_{meta\text{-}C}$ distance in **TS28** is 2.136 Å with C–H and O–H distances of 1.370 and 1.361 Å, respectively.

4. Carbon–carbon bond formation

It has been demonstrated experimentally that the Pd/norbornene-catalyzed reaction of alkyl halides follows the Pd(IV) pathway *via* oxidative addition.[8a,c,17] Further mechanistic study by Lautens and coworkers has proved that the oxidative addition prefers an S_N2 pathway over concerted oxidative addition.[18] A recent experimental/theoretical study on a selective Pd/norbornene-catalyzed trifluoroethylation reaction of indoles by Liu, Lan, and coworkers also supported the S_N2 mechanism for the oxidative addition step.[39] In the case of Pd/norbornene-catalyzed arylation, two possible pathways have been considered for the Pd/norbornene-catalyzed C–C bond formation step: the Pd(II) and Pd(IV) pathways, as depicted in Scheme 3. The Pd(IV) pathway starts with concerted oxidative addition of an aryl halide to the Pd(II) center, followed by the C–C reductive coupling. The Pd(II) pathway undergoes transmetalation with another Pd(II) complex, leading to the formation of dinuclear palladacycle intermediate **VI**. Subsequent C–C reductive elimination leads to the formation of an intermediate **III** with a new C–C bond.

Two possible Pd(IV) pathways starting from five-membered-ring cyclopalladation **30** are investigated first in the present study, as shown in Fig. 6. The ligand dissociation from **30** results in an intermediate **31** with an unsaturated coordination site. The S_N2 mechanism takes place *via* transition state **TS32** with a $\Delta G^{\circ\ddagger}$ of 20.2 kcal mol^{-1}, resulting in a Pd(IV) five-membered-ring intermediate **33**. In the case of the concerted oxidative addition pathway, the unsaturated coordination site near the *meta*-carbon is coordinated by CH_3I to form an intermediate **34**, and then, oxidative addition occurs *via* a three-membered-ring type oxidative addition transition state **TS35** (26.0 kcal mol^{-1}), leading to **33**. Therefore, the S_N2 mechanism is preferred over concerted oxidative addition.[40]

If the intermediate **33** undergoes the C–C reductive coupling first *via* transition state **TS36** (17.3 kcal mol^{-1}) to form an intermediate **37**, in which the *meta*-C is functionalized by the methyl group, the abstraction of iodide from **37** by silver(I) will take place and acetate is bound on the Pd center, generating an intermediate **38**. However, the abstraction of iodide could occur first from **33**, generating an intermediate **39** with an acetate.

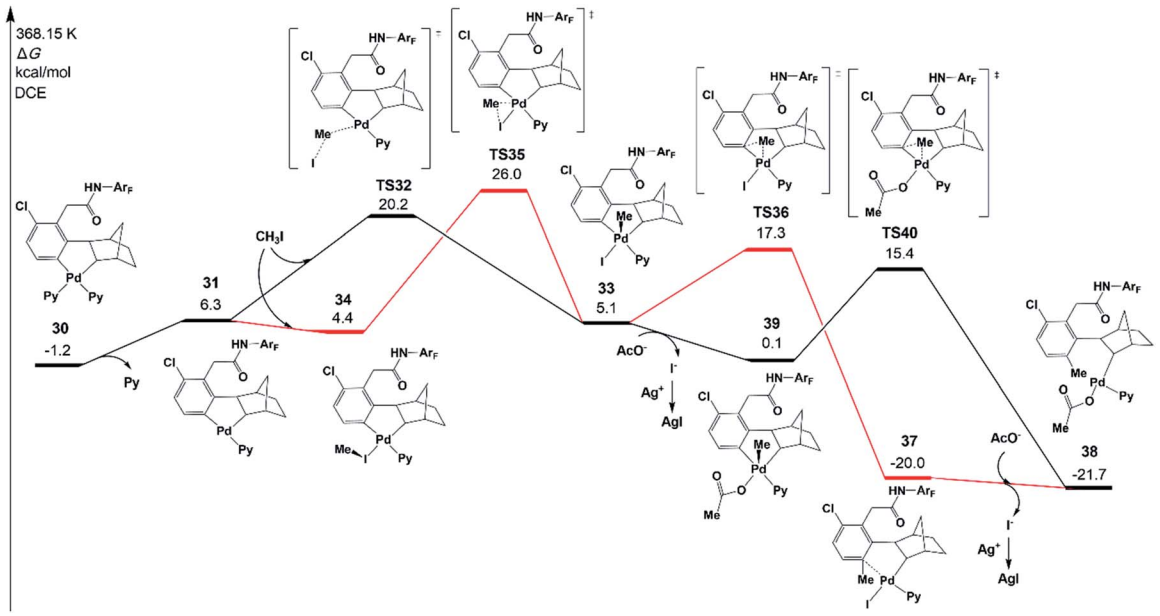

Fig. 6 Gibbs free energy profile for the possible Pd(IV) pathways of the C–C bond formation step.

The subsequent C–C reductive coupling *via* **TS40** needs only 15.4 kcal mol^{-1}, indicating that this pathway is favored.[41]

Fig. 7 presents the free energy profile of the Pd(II) pathway (the transmetalation pathway), which starts with an association intermediate **41** from $CH_3Pd(I)Py_2$ and intermediate **30**. Then, the *meta*-C transfers from the first palladium atom of **41** to the second palladium atom in **43** *via* **TS42**. The reductive elimination occurs *via* **TS44** on the second palladium atom with an energy of 22.4 kcal mol^{-1}.[42,43]

The resulting intermediate **45** could transfer to **36** *via* the release of $Pd(0)Py_2$. The activation energy of the Pd(II) pathway is not so high and $CH_3Pd(I)Py_2$ could be generated from the oxidative addition of $Pd(0)Py_2$ (Scheme 3).[44] However, no Pd(0) species but only the $Pd(II)(OAc)_2$ catalyst was added at the very beginning in the experiments. $Pd(0)Py_2$ could be formed *only if* benzocyclobutene is produced (see Section 6), which is usually unfavoured and occurs at a very late stage. Thus, in the following sections, the activation energy of the Pd(II) pathway *via* **TS43** will be just provided and not be discussed unless the formation of Pd(0) species is preferred.

The key transition states **TS32** and **TS35** of S_N2 and concerted oxidative addition pathways are shown in Fig. 8. **TS32** is a typical S_N2 transition state with a Pd–C–I bond angle of 122.2°. The concerted oxidative addition transition state **TS35** has a three-membered ring with a Pd–C distance of 2.425 Å.

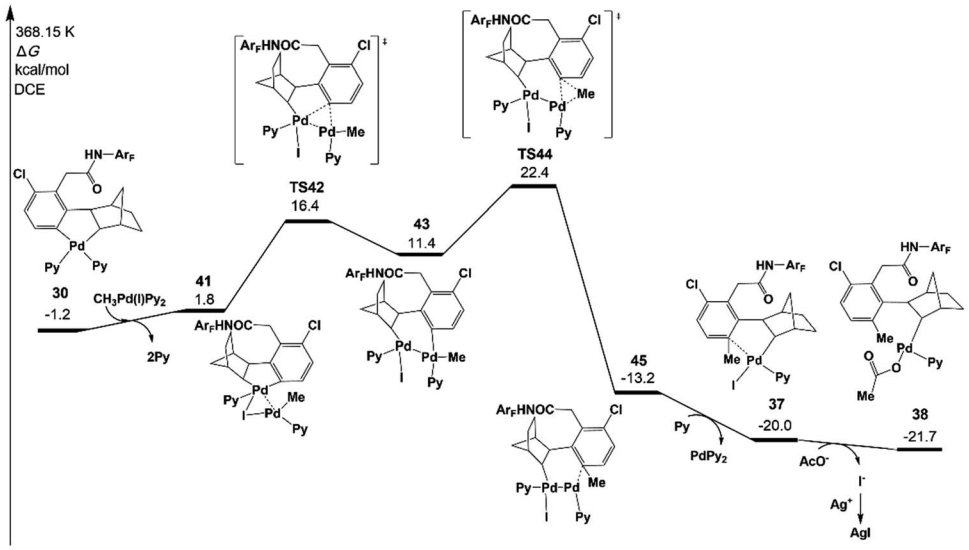

Fig. 7 Gibbs free energy profile for the Pd(II) pathway of the C–C bond formation step.

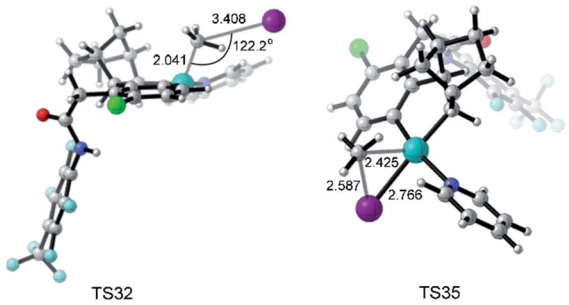

Fig. 8 Optimized structures of transition states **TS32** and **TS35** with selected distances given in angstroms and angles in degrees.

5. β-carbon elimination and protodemetallation

To complete the catalytic cycle, the Pd catalyst has to leave the reaction system to release norbornene and the *meta*-functionalized product, which occurs through β-carbon elimination and protodemetallation. We will first focus on the β-carbon elimination starting from **38**. To obtain the six-membered-ring palladacycle **IV** (Scheme 2), there are two key steps: (a) *ortho*-$C_{norbornene}$ bond cleavage and (b) Pd–N bond formation. Two pathways are possible in terms of the order of those two elementary steps.

In one pathway, the Pd–N bond formation takes place first, as shown in Fig. 9 (black line). *Via* transition state **TS46**, the resultant intermediate **47** was located, which is an eight-membered-ring palladacycle coordinated with acetic acid. The dissociation of acetic acid generates an intermediate **48**. The second step is the β-carbon elimination *via* **TS49** to afford an intermediate **50**. This intermediate undergoes ligand exchange to form six-membered-ring palladacycle **51**. In the other pathway, as shown by the red line in Fig. 9, the *ortho*-$C_{norbornene}$ bond is cleaved *via* transition state **TS52**, followed by the deprotonation reaction (**TS55**) of the amide auxiliary. The highest energy TS in the second pathway is **TS52** (−5.4 kcal mol^{-1}), whose energy is a bit higher than that of **TS49** (−9.6 kcal mol^{-1}) involved in the first pathway. These results demonstrate that the first pathway more preferably occurs than the second one.

The activation energy of norbornene de-insertion *via* **TS49** is as low as 22.7 kcal mol^{-1} relative to **48**, suggesting that it can occur easily under the experimental conditions. On the other hand, the β-H elimination from **38** needs a much larger activation energy of 64.3 kcal mol^{-1}. As mentioned above, the norbornene insertion *via* **TS23** also needs a low activation energy of 22.2 kcal mol^{-1} relative to **14**. The easy norbornene de-insertion, along with norbornene insertion, is of high importance in completing the catalytic *meta*-functionalization reaction.

Fig. 10 depicts free energy profile of the protodemetallation step starting from the intermediate **51**. The protonation reaction occurs on the *meta*-C *via* **TS57** (−11.6 kcal mol^{-1}), leading to an intermediate **58**. This intermediate undergoes acetic acid coordination, protonation of the amide auxiliary, and product dissociation to yield the *meta*-functionalized product **62** with the Pd(II) catalyst. The large activation energy of the above steps is 27.4 kcal mol^{-1} (**TS57** relative to **51**), which is acceptable under the experimental conditions.

6. Formation pathways of three byproducts

Besides the *meta*-functionalized product, three other byproducts could also be generated, as shown in Scheme 2; they are benzocyclobutene, *ortho*-functionalized and *ortho*,*meta*-difunctionalized products. Interestingly, the *meta*-functionalized product and benzocyclobutene were observed experimentally with pyridine-based ligands such as pyridine, **L1**, and **L2**. To disclose the reason for this experimental result, the formation reactions of benzocyclobutene, *ortho*-functionalized and *ortho*,*meta*-difunctionalized products are investigated theoretically in the present work.

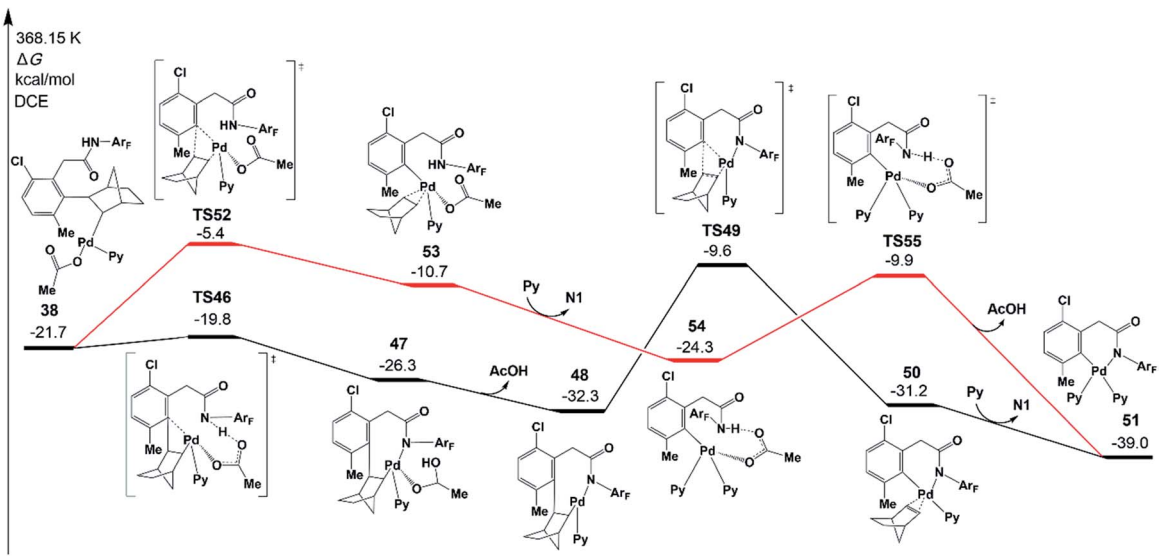

Fig. 9 Gibbs free energy profile for the two possible pathways of β-carbon elimination.

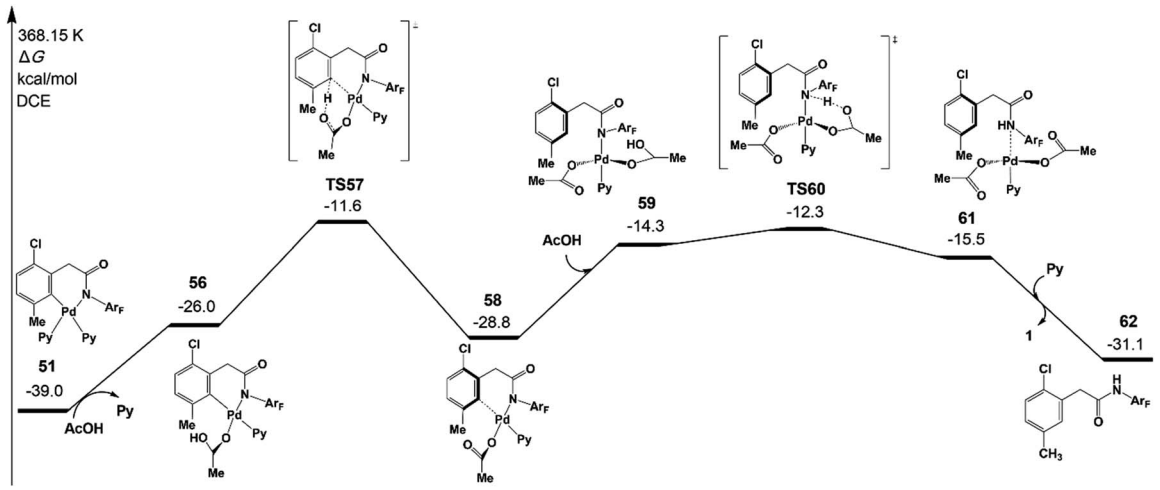

Fig. 10 Gibbs free energy profile for the protodemetallation step of intermediate **51** leading to the *meta*-functionalized product **62**.

As shown in Fig. 11, one possible reaction pathway starting from intermediate **30** is $C_{norborneyl}$–C_{phenyl} bond formation *via* reductive elimination to afford benzocyclobutene **64**. However, the reductive elimination (**TS63**) with two ligands (red line in Fig. 11) needs a large activation energy of 41.2 kcal mol^{-1} relative to **30**. Then, the pathway starting from **31** after the ligand dissociation was examined. The reductive elimination from **31** *via* **TS65** (28.2 kcal mol^{-1}) forms a product complex of benzocyclobutene **66**. The benzocyclobutene **64** will be formed when $PdPy_2$ is dissociated. The possibility of benzocyclobutene formation through the C–C reductive elimination from **33** is also examined. Starting from **32**, the C–C reductive elimination (**TS67**) is 19.0 kcal mol^{-1} in energy and results in benzocyclobutene **64** and $CH_3Pd(I)Py_2$. However, starting from the intermediate **39** that comes from the abstraction of iodide from **33**, the energy barrier of C–C reductive elimination (**TS69**) is only 15.0 kcal mol^{-1}, which is quite close to the activation energy of C–C reductive coupling *via* **TS40** (15.4 kcal mol^{-1}), in excellent agreement with the experimental observation of the same yields of *meta*-functionalization and benzocyclobutene products. $CH_3Pd(OAc)Py_2$ will be generated in this pathway.

Further examinations revealed that the activation energies of the formation pathways of *ortho*-functionalized and *ortho*,*meta*-difunctionalized products are as high as 32.7 and 38.0 kcal

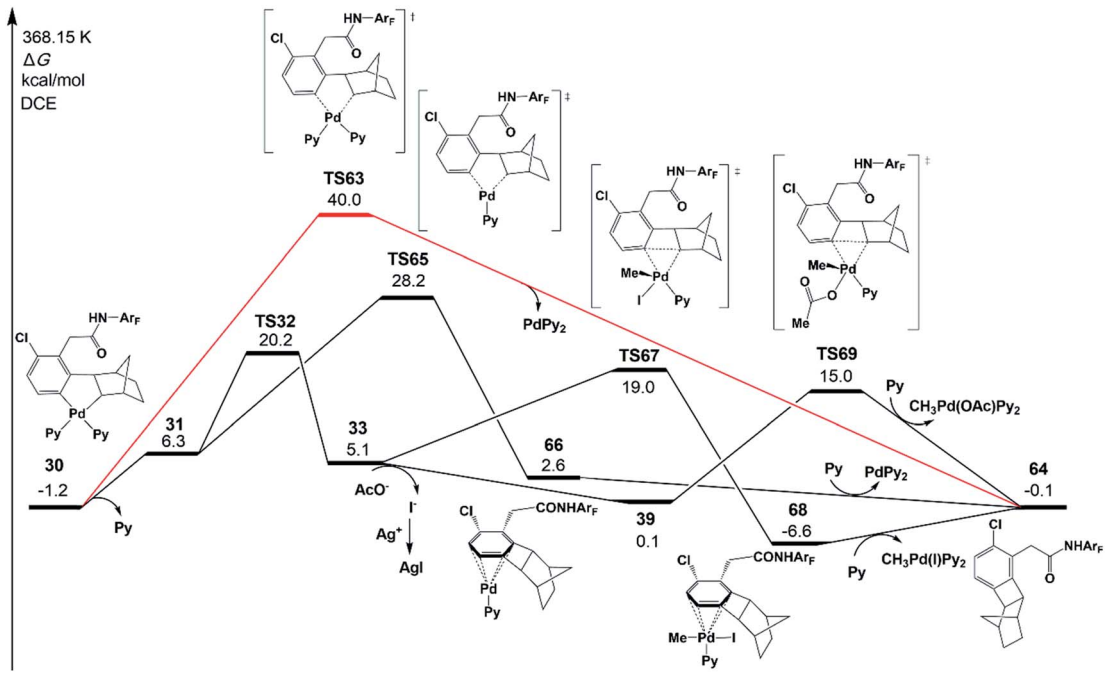

Fig. 11 Gibbs free energy profile for the formation mechanism of the benzocyclobutene product **64** starting from intermediate **30**. Only selected chemical structures are shown for clarity.

mol^{-1}, respectively, suggesting that these pathways could not compete with *meta*-functionalization and benzocyclobutene formation, which agrees well with the experimental observation. Please see Fig. S6 and S7 in the ESI for details.†

7. Ligand and norbornene effects on the selectivity of *meta*-C–H alkylation (or arylation) and benzocyclobutene products

The previous experiments showed that the nature of the ligand, norbornene, and alkyl iodide significantly influence the selectivity between *meta*-functionalized and benzocyclobutene products.[10,11] For the reaction of **1a** with methyl iodide, the *meta*-functionalized product is more favored than benzocyclobutene when **N1** is used as norbornene and either **L1** or **L2** is used as the ligand, but this catalytic system is not effective with ethyl iodide. Further modification of **N1** to **N2** favors the ethylation pathway over the cyclobutene pathway, where **L2** is used as the ligand and **1b** (Scheme 5) is used as the amide substrate. The presence of **N2** also favors other *meta*-alkylation products using various alkyl iodides.

As discussed above, several important steps control the selectivity between *meta*-functionalized and benzocyclobutene products. The Pd(IV) pathway *via* oxidative addition **TS32** (or **TS35**) and the C–C reductive elimination step **TS65** lead to the Pd(IV) intermediate **33** and benzocyclobutene product, respectively. If the Pd(IV) pathway *via* **TS32** (or **TS35**) is preferred over **TS65**, the C–C reductive coupling **TS36** (or **TS40**) and C–C reductive elimination **TS67** (or **TS69**) will become the selectivity-determining steps for *meta*-functionalized and benzocyclobutene products, respectively.

To discuss the ligand effect, the reaction of **1a** with methyl iodide is investigated for consistency with the experiment. As shown in Table 1, the calculated results show excellent agreement with the experimental observation. The concerted oxidative addition pathway *via* **TS35** always could not compete with the S_N2 mechanism *via* **TS32** in the oxidative addition step. Although the catalyst Pd(acridine)$_2$ has possibly been formed together with the benzocyclobutene *via* **TS65**, which would switch on the Pd(II) pathway *via* **TS44** with a low activation energy of 17.4 kcal mol^{-1}, benzocyclobutene formation is still preferred to *meta*-alkylation, revealing that the Pd(IV) pathway and the C–C reductive elimination *via* **TS65** are the dominant pathways under the experimental conditions.

With a small ligand such as Py or DMAP (4-dimethylaminopyridine) as the ligand, the C–C reductive coupling **TS36** (or **TS40**) and C–C reductive elimination **TS67** (or **TS69**) from Pd(IV) intermediate **33** are the selectivity-determining steps. The electron-donating substituent in DMAP stabilizes the Pd(IV) intermediate and further distinguishes the C–C reductive coupling and C–C reductive elimination steps, resulting in the increased yield of *meta*-alkylation. On the other hand, the presence of a large ligand (acridine, **L1**, or **L2**) makes the selectivity-determining step move back to the oxidative addition **TS32** and the C–C reductive elimination **TS65** starting from the Pd(II) intermediate **31**. There are two main reasons: (a) the Pd(IV) intermediate is more sensitive to the ligand size than the Pd(II) intermediate, and thus the C–C reductive elimination from the Pd(IV) intermediate with a large ligand is obviously prohibited; (b) the activation energy of C–C reductive elimination from the Pd(II) intermediate *via* **TS65** remarkably decreases from 28.2–31.3 kcal mol^{-1} with a small ligand to 22.9–24.9 kcal mol^{-1} with a large ligand, which partly comes from the attractive interaction between the large ligand and the 4-$(CF_3)C_6F_4$ group, as shown by the short F–H distance (2.403 Å) in **TS65-N1-L1** in Fig. 12. Further fine tuning of the ligand from acridine to **L1** or **L2** will disfavor the C–C reductive elimination and change the selectivity between *meta*-alkylation and benzocyclobutene formation.

The NBO charges of the Pd atom in **31** were also calculated for all the reaction systems, as shown in Table 1. By comparing the Pd charge with that of acridine (+0.294) and **L2** (+0.294), it is clear that both ligands have similar electron-donating

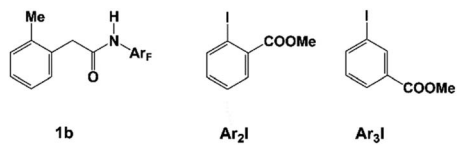

1b **Ar$_2$I** **Ar$_3$I**

Scheme 5 Amide substrate (**1b**), methyl 2-iodobenzoate (**Ar$_2$I**), and methyl 3-iodobenzoate (**Ar$_3$I**).

Table 1 Computed free activation energies $\Delta G^{\circ\ddagger}$ (in kcal mol^{-1}) of the key transition states in *meta*-functionalization and benzocyclobutene formation from amide substrate **1a** and methyl iodide (CH_3I) with several ligands, **N1** as norbornene and DCE as the solvent at 368.15 K. The NBO charges (in |*e*|) of the Pd atom in intermediate **31** are also provided[45]

	Charges	Pd(IV) pathway				*meta*-Methylation		Benzocyclobutene			Pd(II) pathway	Experimental yields[10]
	Pd in **31**	**TS32**	**TS35**	**TS65**	$\Delta\Delta G^{\circ\ddagger}$(a)[a]	**TS36**	**TS40**	**TS67**	**TS69**	$\Delta\Delta G^{\circ\ddagger}$(b)[b]	**TS44**	*meta*-Methylation:benzocyclobutene
Py	+0.329	20.2	26.0	28.2	**−8.0**	17.3	15.4	19.0	15.0	**+0.4**	22.4	15%:15%
DMAP	+0.314	23.9	30.5	31.3	**−7.4**	19.4	18.7	23.0	21.3	**−2.6**	35.5	32%:8%
Acridine	+0.294	23.4	30.2	22.9	**+0.5**	11.0	13.8	13.7	15.6	**−2.7**	17.4	28%:58%
L1	+0.286	23.3	31.1	24.5	**−1.2**	10.1	14.2	14.7	15.0	**−4.6**	28.3	85%:15%
L2	+0.294	24.0	33.4	24.9	**−0.9**	10.7	7.3	15.6	13.9	**−6.6**	23.3	80%:20%

[a] $\Delta\Delta G^{\circ\ddagger}$(a) = $\Delta\Delta G^{\circ\ddagger}$(**TS32**–**TS65**). [b] $\Delta\Delta G^{\circ\ddagger}$(b) = $\Delta\Delta G^{\circ\ddagger}$(min{**TS36**,**TS40**}–min{**TS67**,**TS69**}).

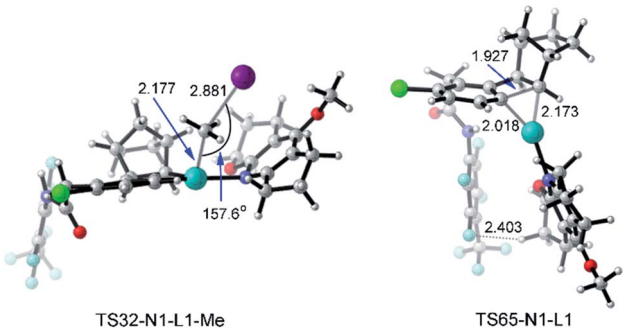

Fig. 12 Optimized structures of transition states **TS32-N1-L1-Me** and **TS65-N1-L1** of methyl iodide. The selected distances and angles are given in angstroms and in degrees, respectively.

properties; however, the selectivity between the C–C reductive coupling and C–C reductive elimination is reversed from acridine to **L2**, indicating that both geometric and electronic properties of the ligand play important roles.

Fig. 12 presents the optimized structures of transition states **TS32-N1-L1-Me** and **TS65-N1-L1** with **L1** as the ligand, which are the selectivity-determining steps. **TS32-N1-L1-Me** is a typical S_N2 transition state with a Pd–C–I angle of 157.6°. The F–H distance of 2.403 Å in **TS65-N1-L1** is shorter than the sum of van der Waals radii of hydrogen (1.10 Å) and fluorine (1.46 Å),[46] suggesting the attractive interaction between the ligand and 4-(CF_3)C_6F_4 group.

For the norbornene effect on *meta*-alkylation, the reaction of **1b** with ethyl iodide is studied using **N1**, **N2** and **L2** as the ligand, considering experimental conditions. As shown in Table 2, when norbornene **N1** is employed, the oxidative addition step *via* **TS32** is moderately lower in energy (−1.7 kcal mol^{-1}) than the C–C reductive elimination step *via* **TS65**; however, the reductive coupling *via* **TS36** is disfavored by 0.6 kcal mol^{-1} in energy than the C–C reductive coupling *via* **TS67**. This result agrees with the experimental observation that the yields of benzocyclobutene and the *meta*-ethylation products are 85% *vs.* 10%.

When **N2** is used instead of **N1**, the C–C reductive elimination steps, including **TS65**, **TS67**, and **TS69**, need higher activation energies, leading to an obvious energy difference of 7.5 kcal mol^{-1} (or 11.8 kcal mol^{-1}) between **TS32** (or **TS40**) and **TS65** (or **TS69**). These results clearly reveal that with **N2** as norbornene the *meta*-ethylation product is preferred over benzocyclobutene, consistent with the experimental result. Because of the repulsion induced by the CO_2Me group in **N2**, the C–C reductive elimination is prohibited, which was also found in our recent theoretical study on Ni-catalyzed (2 + 2 + 2) cycloaddition of 1,6-ene-allenes and alkenes.[47] As shown in Fig. 13, the steric repulsion in **TS40-N1-L2-Et** mainly appears between the ethyl group and substrate (or norbornene), as indicated by the two short H–H distances (2.263 and 2.288 Å). Nevertheless, in **TS40-N2-L2-Et**, several short H–H distances appear, including 2.217, 2.456, and 2.475 Å, indicating the obvious steric repulsion. The NBO charge of the Pd atom in **31** as shown in Table 2 increases from +0.285 with **N1** to +0.356 with **N2**, which comes from the electron-withdrawing property of the CO_2Me group. The presence of the CO_2Me group also favors the S_N2 pathway *via* **TS32** with the activation energy slightly decreasing from 23.2 to 22.7 kcal mol^{-1} and concerted oxidative addition *via* **TS35** with the activation energy dropping from 27.6 to 23.1 kcal mol^{-1}.[45]

Besides *meta*-alkylation, *meta*-arylation producing biaryl compounds can also be achieved with the catalytic systems **A** (**L1** and **N1**) and **B** (**L2** and **N2**). Compared to the catalytic system **A** which is only effective for *ortho*-substituted aryl iodides, catalytic system **B** in $PhCF_3$ solvent has been successfully applied to *meta*-arylation of phenyl iodide and 2-, 3- or 4-substituted aryl iodides.[10,11,48] Thus, the key selectivity-

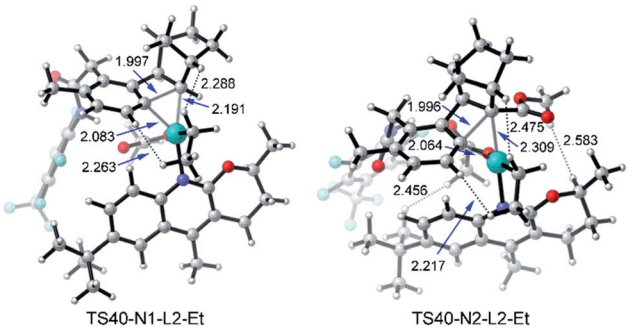

Fig. 13 Optimized structures of transition states **TS40-N1-L2-Et** and **TS40-N2-L2-Et** of amide substrate **1b** and ethyl iodide with the selected distances given in angstroms.

Table 2 Computed free activation energies $\Delta G^{\circ\ddagger}$ (in kcal mol^{-1}) of the key transition states in *meta*-functionalization and benzocyclobutene formation from amide substrate **1b** and ethyl iodide (C_2H_5I) with norbornenes (**N1** and **N2**), **L2** as the ligand and DCE as the solvent at 348.15 K. The NBO charges (in |e|) of the Pd atom in intermediate **31** are also provided[45]

	Charges	Pd(IV) pathway				*meta*-Ethylation		Benzocyclobutene			Pd(II) pathway	Experimental yields[11]
	Pd in **31**	**TS32**	**TS35**	**TS65**	$\Delta\Delta G^{\circ\ddagger}$(a)[a]	**TS36**	**TS40**	**TS67**	**TS69**	$\Delta\Delta G^{\circ\ddagger}$(b)[b]	**TS44**	*meta*-Ethylation:benzocyclobutene
N1	+0.285	23.2	27.6	24.9	**−1.7**	13.6	15.0	13.0	15.4	**+0.6**	21.3	10%:85%
N2	+0.356	22.7	23.1	30.2	**−7.5**	23.1	19.5	33.7	31.4	**−11.9**	30.8	97%:0%

[a] $\Delta\Delta G^{\circ\ddagger}$(a) = $\Delta\Delta G^{\circ\ddagger}$(**TS32**–**TS65**). [b] $\Delta\Delta G^{\circ\ddagger}$(b) = $\Delta\Delta G^{\circ\ddagger}$(min{**TS36**,**TS40**}–min{**TS67**,**TS69**}).

Table 3 Computed activation energies $\Delta G^{\circ\ddagger}$ (in kcal mol^{-1}) of the key transition states in *meta*-functionalization and benzocyclobutene formation from amide substrate **1b** and aryl iodides Ar_2I or Ar_3I with **L2**, **N2**, and $PhCF_3$ (solvent) at 363.15 K[45]

	Pd(IV) pathway			*meta*-Arylation		Benzocyclobutene			Pd(II) pathway	Experimental yields[10,11]
	TS35	**TS65**	$\Delta\Delta G^{\circ\ddagger}$(a)[a]	**TS36**	**TS40**	**TS67**	**TS69**	$\Delta\Delta G^{\circ\ddagger}$(b)[b]	**TS44**	*meta*-Arylation: benzocyclobutene
Ar_2I	**28.7**	34.9	**−6.2**	26.8	21.0	34.6	29.1	**−8.1**	37.3	100%:0%
Ar_3I	**30.0**	34.9	**−4.9**	24.3	17.7	39.5	34.7	**−17.0**	30.2	100%:0%

[a] $\Delta\Delta G^{\circ\ddagger}$(a) = $\Delta\Delta G^{\circ\ddagger}$(**TS35**–**TS65**). [b] $\Delta\Delta G^{\circ\ddagger}$(b) = $\Delta\Delta G^{\circ\ddagger}$(min{**TS36**,**TS40**}–min{**TS67**,**TS69**}).

determining steps were investigated by employing the catalytic system **B** with amide substrate **1b** and methyl 2-iodobenzoate Ar_2I (or methyl 3-iodobenzoate Ar_3I, Scheme 5) as the reactant model. Since the concerted oxidative addition transition state has been revealed to be preferred for aryl iodides in the Pd(IV) pathway,[20] the S_N2 pathway *via* **TS32** will not be discussed here.

Table 3 shows the computed activation energies of all the selected transition states. The selectivity-determining step is the oxidative addition *via* **TS35** and C–C reductive elimination *via* **TS65**. For both Ar_2I and Ar_3I, the activation energy for **TS35** is obviously lower than that of **TS65**, which agrees with the experimental observation that catalytic system **B** is effective for both *ortho*-substituted and *ortho*-unsubstituted aryl iodides. However, *ortho*-substituted aryl iodide is more easily coupled than *ortho*-unsubstituted aryl iodide because of the lower activation energy (28.7 kcal mol^{-1}) for oxidative addition with Ar_2I than that (30.0 kcal mol^{-1}) with Ar_3I, which might be attributed to the attractive interaction between the directing group and CO_2Me of Ar_2I, as indicated by the short O–H distance (2.059 Å) in Fig. 14. The Pd(IV) pathway *via* **TS44** does not play an important role, since Pd(**L2**)$_2$ could not be generated under the experimental conditions. The activation energy (30.2 kcal mol^{-1}) for **TS44** with Ar_3I is comparable to that of **TS35**, indicating that the combination of a large ligand and modified norbornene can make the Pd(IV) pathway have similar activation energy, although there is an *ortho*-substituted group (the directing group) of the phenyl group.

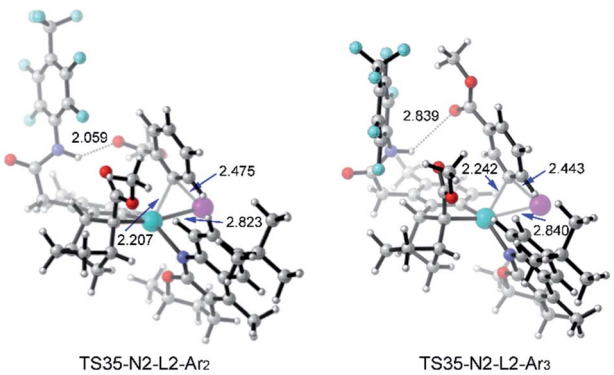

Fig. 14 Optimized structures of TS35-N2-L2-Ar2 and T35-N2-L3-Ar_3 of amide substrate **1b** and aryl iodide (Ar_2I and Ar_3I) with selected distances given in angstroms.

Conclusions

We have theoretically investigated the detailed mechanism, norbornene and ligand effects, and origins of selectivity in a newly developed Pd/norbornene-catalyzed *meta*-selective C–H activation and alkylation. The reaction starts initially with the substrate binding to the Pd(II) center through an amidate auxiliary, followed by the *ortho*-C–H activation *via* a CMD mechanism, which generates the six-membered-ring cyclopalladate(II) intermediate. This Pd(II) intermediate further undergoes norbornene insertion and *meta*-C–H activation *via* a CMD mechanism, forming the five-membered-ring cyclopalladate(II) intermediate. The subsequent *meta*-functionalization step adopts the Pd(IV) pathway *via* oxidative addition and C–C reductive coupling rather than the Pd(II) pathway *via meta*-C–C reductive coupling on dinuclear palladium species because of the low concentration of Pd(0)L_2. Finally, to complete the catalytic cycle, norbornene dissociation takes place followed by protodemetallation with the formation of a six-membered-ring palladacycle(**II**) intermediate.

There are two possible pathways for the oxidative addition step, which depends on the nature of the coupling iodide; the alkyl iodide undergoes an S_N2 pathway, whereas the aryl iodide prefers concerted oxidative addition rather than the S_N2 pathway. For methyl iodide, with norbornene and pyridine (or DMAP), the C–C reductive coupling and C–C reductive elimination from the Pd(IV) intermediate are found to be the selectivity-determining steps of *meta*-functionalization and benzocyclobutene formation, respectively. However, the use of a large ligand (acridine, **L1**, and **L2**) changes the selectivity-determining step to the oxidative addition and the C–C reductive elimination from the Pd(II) intermediate. The geometric and electronic properties of **L1** and **L2** suppress the benzocyclobutene formation by increasing the energy difference between those two pathways. The combination of 2-carbomethoxynorbornene and **L2** utilizes the electronic and steric effects and promotes *meta*-alkylation and -arylation by disfavoring the C–C reductive elimination steps from the Pd(II) and Pd(IV) intermediates as well as favoring the oxidative addition step.

Conflicts of interest

There are no conflicts to declare.

Acknowledgements

T. Y. acknowledges the "Young Talent Support Plan" of Xi'an Jiaotong University. M. E. acknowledges the financial support from a Grant-in-Aid for Scientific Research from the Japan Society for the Promotion of Science (JSPS) (JP16H06511, JPH04104) and the Nanotechnology Platform Program (Molecule and Material Synthesis) of the Ministry of Education, Culture, Sports, Science, and Technology (MEXT) of Japan. This work was also supported by the Joint Funds of the National Natural Science Foundation and China-State Grid Corporation (U1866203), the Fundamental Research Funds for the Central Universities and the World-Class Universities (Disciplines) and the Characteristic Development Guidance Funds for the Central Universities. DFT calculations were partially performed at the HPC Platform of Xi'an Jiaotong University, China and the Research Center for Computational Science, Okazaki, Japan. We are also grateful to Prof. Shigeyoshi Sakaki (Kyoto University) and Prof. Jin-Quan Yu (The Scripps Research Institute) for numerous fruitful discussions.

Notes and references

1 (*a*) D. A. Petrone, J. Ye and M. Lautens, *Chem. Rev.*, 2016, **116**, 8003; (*b*) J. J. Topczewskia and M. S. Sanford, *Chem. Sci.*, 2015, **6**, 70; (*c*) H. M. L. Davies and D. Morton, *J. Org. Chem.*, 2016, **81**, 343; (*d*) Z. Dong, Z. Ren, S. J. Thompson, Y. Xu and G. Dong, *Chem. Rev.*, 2017, **117**, 9333.

2 (*a*) N. Della Ca', M. Fontana, E. Motti and M. Catellani, *Acc. Chem. Res.*, 2016, **49**, 1389; (*b*) G. Song and X. Li, *Acc. Chem. Res.*, 2015, **48**, 1007; (*c*) J. Yang, *Org. Biomol. Chem.*, 2015, **13**, 1930; (*d*) J. Ye and M. Lautens, *Nat. Chem.*, 2015, **7**, 863; (*e*) J. Ye, Z. Shi, T. Sperger, Y. Yasukawa, C. Kingston, F. Schoenebeck and M. Lautens, *Nat. Chem.*, 2017, **9**, 361; (*f*) J. Wang, R. Li, Z. Dong, P. Liu and G. Dong, *Nat. Chem.*, 2018, **10**, 866.

3 (*a*) Y. Kuninobu, H. Ida, M. Nishi and M. Kanai, *Nat. Chem.*, 2015, **7**, 712; (*b*) M. Bera, S. Agasti, R. Chowdhury, R. Mondal, D. Pal and D. Maiti, *Angew. Chem., Int. Ed.*, 2017, **56**, 5272; (*c*) X.-Y. Chen and E. J. Sorensen, *Chem. Sci.*, 2018, **9**, 8951; (*d*) Z. Fan, J. Ni and A. Zhang, *J. Am. Chem. Soc.*, 2016, **138**, 8470; (*e*) T. Patra, S. Bag, R. Kancherla, A. Mondal, A. Dey, S. Pimparkar, S. Agasti, A. Modak and D. Maiti, *Angew. Chem., Int. Ed.*, 2016, **55**, 7751; (*f*) M.-Z. Lu, X.-R. Chen, H. Xu, H.-X. Dai and J.-Q. Yu, *Chem. Sci.*, 2018, **9**, 1311; (*g*) S. Okumura, S. Tang, T. Saito, K. Semba, S. Sakaki and Y. Nakao, *J. Am. Chem. Soc.*, 2016, **138**, 14699; (*h*) B. Ma, Z. Chu, B. Huang, Z. Liu, L. Liu and J. Zhang, *Angew. Chem., Int. Ed.*, 2017, **56**, 2749; (*i*) M. E. Hoque, R. Bisht, C. Haldar and B. Chattopadhyay, *J. Am. Chem. Soc.*, 2017, **139**, 7745; (*j*) A. Unnikrishnana and R. B. Sunoj, *Chem. Sci.*, 2019, **10**, 3826.

4 (*a*) M. Ye, G.-L. Gao and J.-Q. Yu, *J. Am. Chem. Soc.*, 2011, **133**, 6964; (*b*) K. L. Hull and M. S. Sanford, *J. Am. Chem. Soc.*, 2007, **129**, 11904.

5 (*a*) J. Luo, S. Preciado and I. Larrosa, *J. Am. Chem. Soc.*, 2014, **136**, 4109; (*b*) M. Font, A. R. A. Spencer and I. Larrosa, *Chem. Sci.*, 2018, **9**, 7133; (*c*) J. Cornella, M. Righi and I. Larrosa, *Angew. Chem., Int. Ed.*, 2011, **50**, 9429.

6 (*a*) R. J. Phipps and M. J. Gaunt, *Science*, 2009, **323**, 1593; (*b*) H. A. Duong, R. E. Gilligan, M. L. Cooke, R. J. Phipps and M. J. Gaunt, *Angew. Chem., Int. Ed.*, 2011, **50**, 463; (*c*) S. Li, H. Ji, L. Cai and G. Li, *Chem. Sci.*, 2015, **6**, 5595; (*d*) S. Li, L. Cai, H. Ji, L. Yang and G. Li, *Nat. Commun.*, 2016, **7**, 10443.

7 (*a*) D. Leow, G. Li, T.-S. Mei and J.-Q. Yu, *Nature*, 2012, **486**, 518; (*b*) R.-Y. Tang, G. Li and J.-Q. Yu, *Nature*, 2014, **507**, 215; (*c*) Y.-F. Yang, G.-J. Cheng, P. Liu, D. Leow, T.-Y. Sun, P. Chen, X. Zhang, J.-Q. Yu, Y.-D. Wu and K. N. Houk, *J. Am. Chem. Soc.*, 2014, **136**, 344; (*d*) A. Maji, B. Bhaskararao, S. Singha, R. B. Sunoj and D. Maiti, *Chem. Sci.*, 2016, **7**, 3147.

8 (*a*) M. Catellani, F. Frignani and A. Rangoni, *Angew. Chem., Int. Ed. Engl.*, 1997, **36**, 119; (*b*) M. Lautens and S. Piguel, *Angew. Chem., Int. Ed.*, 2000, **39**, 1045; (*c*) A. Martins, B. Mariampillai and M. Lautens, *Top. Curr. Chem.*, 2010, **292**, 1–33.

9 (*a*) L. Jiao and T. Bach, *J. Am. Chem. Soc.*, 2011, **133**, 12990; (*b*) L. Jiao, E. Herdtweck and T. Bach, *J. Am. Chem. Soc.*, 2012, **134**, 14563; (*c*) J. Wang and G. Dong, *Chem. Rev.*, 2019, **119**, 7478.

10 X.-C. Wang, W. Gong, L.-Z. Fang, R.-Y. Zhu, S. Li, K. M. Engle and J.-Q. Yu, *Nature*, 2015, **519**, 334.

11 P.-X. Shen, X.-C. Wang, P. Wang, R.-Y. Zhu and J.-Q. Yu, *J. Am. Chem. Soc.*, 2015, **137**, 11574.

12 (*a*) Q. Ding, S. Ye, G. Cheng, P. Wang, M. E. Farmer and J.-Q. Yu, *J. Am. Chem. Soc.*, 2017, **139**, 417; (*b*) P. Wang, G.-C. Li, P. Jain, M. E. Farmer, J. He, P. X. Shen and J.-Q. Yu, *J. Am. Chem. Soc.*, 2016, **138**, 14092; (*c*) P. Wang, M. E. Farmer, X. Huo, P. Jain, P.-X. Shen, M. Ishoey, J. E. Bradner, S. R. Wisniewski, M. D. Eastgate and J.-Q. Yu, *J. Am. Chem. Soc.*, 2016, **138**, 9269; (*d*) H. Shi, P. Wang, S. Suzuki, M. E. Farmer and J.-Q. Yu, *J. Am. Chem. Soc.*, 2016, **138**, 14876; (*e*) P. Wang, M. E. Farmer and J.-Q. Yu, *Angew. Chem., Int. Ed.*, 2017, **56**, 5125; (*f*) G.-C. Li, P. Wang, M. E. Farmer and J.-Q. Yu, *Angew. Chem., Int. Ed.*, 2017, **56**, 6874; (*g*) G. Cheng, P. Wang and J.-Q. Yu, *Angew. Chem., Int. Ed.*, 2017, **56**, 8183.

13 Z. Dong, J. Wang and G. Dong, *J. Am. Chem. Soc.*, 2015, **137**, 5887.

14 H. Shi, A. N. Herron, Y. Shao, Q. Shao and J.-Q. Yu, *Nature*, 2018, **558**, 581.

15 (*a*) F. Ozawa, M. Fujimori, T. Yamamoto and A. Yamamoto, *Organometallics*, 1986, **5**, 2144; (*b*) F. Ozawa, T. Hidaka, T. Yamamoto and A. Yamamoto, *J. Organomet. Chem.*, 1987, **330**, 253; (*c*) Y. Suzaki, T. Yagyu, Y. Yamamura, A. Mori and K. Osakada, *Organometallics*, 2002, **21**, 5254.

16 D. J. Cardenas, B. Martin-Matute and A. M. Echavarren, *J. Am. Chem. Soc.*, 2006, **128**, 5033.

17 (*a*) M. Catellani and G. P. Chiusoli, *J. Organomet. Chem.*, 1988, **346**, C27; (*b*) M. Catellani and M. C. Fagnola, *Angew. Chem., Int. Ed.*, 1995, **33**, 2421; (*c*) A. Dedieu and A. J. Mota, *Can. J. Chem.*, 2009, **87**, 838.

18 A. Rudolph, N. Rackelmann and M. Lautens, *Angew. Chem., Int. Ed.*, 2007, **46**, 1485.

19 Q. Liu, Y. Lan, J. Liu, G. Li, Y. D. Wu and A. Lei, *J. Am. Chem. Soc.*, 2009, **131**, 10201.
20 G. Maestri, E. Motti, N. Della Ca', M. Malacria, E. Derat and M. Catellani, *J. Am. Chem. Soc.*, 2011, **133**, 8574.
21 J. D. Chai and M. Head-Gordon, *Phys. Chem. Chem. Phys.*, 2008, **10**, 6615.
22 (*a*) P. J. Hay and W. R. Wadt, *J. Chem. Phys.*, 1985, **82**, 270; (*b*) P. J. Hay and W. R. Wadt, *J. Chem. Phys.*, 1985, **82**, 299.
23 Y. Zhao and D. G. Truhlar, *Theor. Chem. Acc.*, 2008, **120**, 215.
24 (*a*) A. D. Becke, *Phys. Rev. A*, 1988, **38**, 3098; (*b*) C. T. Lee, W. T. Yang and R. G. Parr, *Phys. Rev. B: Condens. Matter Mater. Phys.*, 1988, **37**, 785; (*c*) S. Grimme, *J. Comput. Chem.*, 2004, **25**, 1463; (*d*) S. Grimme, S. Ehrlich and L. Goerigk, *J. Comput. Chem.*, 2011, **32**, 1456.
25 Test calculations were performed on the key intermediates and transition states. Different functionals and basis sets used in optimization and single-point energy calculations gave similar results. Please see the results and discussion in Fig. S14 and Table S1 in the ESI.†
26 D. Andrae, U. Häusermann, M. Dolg, H. Stoll and H. Preus, *Theor. Chim. Acta*, 1990, **77**, 123.
27 (*a*) Y. Minenkov, Å. Singstad, G. Occhipinti and V. R. Jensen, *Dalton Trans.*, 2012, **41**, 5526; (*b*) T. Sperger, I. A. Sanhueza, I. Kalvet and F. Schoenebeck, *Chem. Rev.*, 2015, **115**, 9532; (*c*) L. Fang, T. G. Saint-Denis, B. L. H. Taylor, S. Ahlquist, K. Hong, S. Liu, L. Han, K. N. Houk and J.-Q. Yu, *J. Am. Chem. Soc.*, 2017, **139**, 10702; (*d*) Y.-F. Yang, G. Chen, X. Hong, J.-Q. Yu and K. N. Houk, *J. Am. Chem. Soc.*, 2017, **139**, 8514; (*e*) H. Zheng, K. Semba, Y. Nakao and S. Sakaki, *J. Am. Chem. Soc.*, 2017, **139**, 14065.
28 A. V. Marenich, C. J. Cramer and D. G. Truhlar, *J. Phys. Chem. B*, 2009, **113**, 6378.
29 In SMD calculations, the dielectric constant and the solute volume of $PhCF_3$ were set as 9.18 and 4.06 angstroms, respectively.
30 E. D. Glendening, A. E. Reed, J. E. Carpenter and F. Weinhold, *NBO, version 3.1*, University of Wisconsin, Madison, WI, 1996.
31 M. J. Frisch, G. W. Trucks, H. B. Schlegel, G. E. Scuseria, M. A. Robb, J. R. Cheeseman, G. Scalmani, V. Barone, B. Mennucci, G. A. Petersson, H. Nakatsuji, M. Caricato, X. Li, H. P. Hratchian, A. F. Izmaylov, J. Bloino, G. Zheng, J. L. Sonnenberg, M. Hada, M. Ehara, K. Toyota, R. Fukuda, J. Hasegawa, M. Ishida, T. Nakajima, Y. Honda, O. Kitao, H. Nakai, T. Vreven, J. A. Montgomery Jr, J. E. Peralta, F. Ogliaro, M. Bearpark, J. J. Heyd, E. Brothers, K. N. Kudin, V. N. Staroverov, T. Keith, R. Kobayashi, J. Normand, K. Raghavachari, A. Rendell, J. C. Burant, S. S. Iyengar, J. Tomasi, M. Cossi, N. Rega, J. M. Millam, M. Klene, J. E. Knox, J. B. Cross, V. Bakken, C. Adamo, J. Jaramillo, R. Gomperts, R. E. Stratmann, O. Yazyev, A. J. Austin, R. Cammi, C. Pomelli, J. W. Ochterski, R. L. Martin, K. Morokuma, V. G. Zakrzewski, G. A. Voth, P. Salvador, J. J. Dannenberg, S. Dapprich, A. D. Daniels, O. Farkas, J. B. Foresman, J. V. Ortiz, J. Cioslowski and D. J. Fox, *Gaussian 09, Revision E.01*, Gaussian, Inc., Wallingford, CT, 2013.
32 C. Y. Legault, *CYLView, 1.0b*, Universitéde Sherbrooke, Canada, 2009, http://www.cylview.org.
33 J. He, S. Li, Y. Q. Deng, H. Fu, B. N. Laforteza, J. E. Spangler, A. Homs and J.-Q. Yu, *Science*, 2014, **343**, 1216.
34 Y. Dang, S. Qu, J. W. Nelson, H. D. Pham, Z.-X. Wang and X. Wang, *J. Am. Chem. Soc.*, 2015, **137**, 2006.
35 (*a*) S. Winstein and T. G. Traylor, *J. Am. Chem. Soc.*, 1955, **77**, 3747; (*b*) L. Ackermann, *Chem. Rev.*, 2011, **111**, 1315; (*c*) B. Biswas, M. Sugimoto and S. Sakaki, *Organometallics*, 2000, **19**, 3895; (*d*) W. Guan, F. B. Sayyed, G. Zeng and S. Sakaki, *Inorg. Chem.*, 2014, **53**, 6444.
36 The direct-CMD will produce the intermediate **18** directly.
37 The transition state of the second norbornene insertion into 30 needs a much higher activation energy (69.2 kcal mol^{-1}). Please see Fig. S8 in the ESI.†.
38 The *endo*-migratory insertion of norbornene *via* **TS23′** needs a higher activation energy of 30.2 kcal mol^{-1}.
39 H. Zhang, H.-Y. Wang, Y. Luo, C. Chen, Y. Cao, P. Chen, Y.-L. Guo, Y. Lan and G. Liu, *ACS Catal.*, 2018, **8**, 2173.
40 The phenomenon that the S_N2 pathway is more favoured than the concerted oxidative addition was also found in the experimental/theoretical study on the Ni-catalyzed coupling reaction of alkyl halides with aryl Grignard reagents in the presence of 1,3-butadiene, see T. Iwasaki, A. Fukuoka, W. Yokoyama, X. Min, I. Hisaki, T. Yang, M. Ehara, H. Kuniyasua and N. Kambe, *Chem. Sci.*, 2018, **9**, 2195.
41 Possible transition states for the C_{methyl}–$C_{norbornene}$ reductive coupling starting from **33** have been examined. The activation energy of those transition states is at least 22.6 kcal mol^{-1}, which is obviously higher than those of **TS36**, **TS40**, **TS66**, and **TS68** (Fig. S9 in the ESI†).
42 Other possible transition state structures of **TS44** with two (or three) ligands have been examined; however, their activation energies are higher than that of **TS44** (Fig. S10†).
43 The transition state for the C_{methyl}–$C_{norbornene}$ reductive coupling starting from **43** needs an activation energy of 32.2 kcal mol^{-1}, which is higher than that of **TS44** (Fig. S10†).
44 The oxidative addition of CH_3I on $PdPy_2$, which gives rise to $CH_3Pd(I)Py_2$, needs an acceptable activation energy of 26.0 kcal mol^{-1}. Please see Fig. S11 in the ESI.†.
45 In Tables 1–3, complex **1** is taken as the energy reference point. If the intermediate **30** is taken as the energy reference point, the activation energies for the **TS32** in Table 2 are 24.8 and 27.0 kcal mol^{-1} for **N1** and **N2**, respectively, which agrees with the fact that positive charge would disfavor the S_N2 pathway.
46 R. S. Rowland and R. Taylor, *J. Phys. Chem.*, 1996, **100**, 7384.
47 T. Yang and M. Ehara, *J. Org. Chem.*, 2017, **82**, 2150.
48 By tuning directing groups and ligands, *meta*-arylation has also been reported for *ortho*-unsubstituted aryl iodides by using Pd and simple norbornene. Please see ref. 12a and J. Han, L. Zhang, Y. Zhu, Y. Zheng, X. Chen, Z.-B. Huang, D.-Q. Shi and Y. Zhao, *Chem. Commun.*, 2016, **52**, 6903.